Deep Learning Enabled Rapid Nonlinear Time History Wind Performance Assessment

Bowei Li<sup>a</sup>, Seymour M.J. Spence<sup>a,1,\*</sup>

<sup>a</sup>Department of Civil and Environmental Engineering, University of Michigan, Ann Arbor, MI 48109, USA

Abstract

The ever-growing interest in performance-based wind engineering (PBWE) can be traced back to the potential to deliver more rational and economical designs. The computational effort involved in the probabilistic performance assessments underpinning PBWE is, however, a major barrier to wider applicability. This is especially true in light of the reliance of PBWE on nonlinear dynamic analysis. This work is centered on alleviating this barrier through the development of a deep learning metamodeling technique for rapidly predicting the nonlinear dynamic response of structural systems subject to stochastic wind loads. The metamodeling technique is based on first identifying a reduced space by Galerkin projection that is subsequently learned through the application of long short-term memory (LSTM) neural networks. Methods are proposed that enable the training of the deep learning metamodel to multiple wind directions using short-duration segments of nonlinear dynamic response time histories. The potential of the framework is demonstrated through application to a 37-story steel frame modeled with fiber-based distributed plasticity and subject to stochastic wind excitation. The calibrated deep learning metamodel is seen to be capable of accurately simultaneously reproducing both the displacement and fiber response at all degrees of freedom with speedups of over four orders of magnitude.

Keywords: Metamodeling, Deep learning, Nonlinear dynamic wind response, Probabilistic wind performance assessment

Email addresses: jacklbw@umich.edu (Bowei Li), smjs@umich.edu (Seymour M.J. Spence)

<sup>\*</sup>Corresponding author

 $<sup>^{1}</sup>$ Tel. +1-734-764-8419, Fax +1-734-764-4292

#### 1. Introduction

Performance-based wind engineering (PBWE) has gained significant attention over the last two decades as a methodology for rationally ensuring predetermined performance goals are met by designs that offer increased safety at reduced costs. Significant research has been devoted to the development of frameworks for the implementation of PBWE, e.g., [1, 2, 3, 4, 5, 6, 7, 8, 9]. These efforts have resulted in great interest from industry for the implementation in practice of PBWE leading to the recent publication by the American Society of Civil Engineers of the Prestandard for Performance-Based Wind Design [10]. One of the key concepts that has emerged for implementing PBWE is the need for performance evaluations supported by nonlinear dynamic response analysis.

Notwithstanding the significant computational cost, direct integration is generally considered for the estimation of the nonlinear dynamic response [11, 12, 13, 14, 15, 16], To overcome the massive computational burden associated with integrating over the long duration of typical windstorms, in the order of hours, more efficient methods have been prospered including static pushover analysis [17, 12], dynamic shakedown [18, 19], and reduced models [20, 21]. Nevertheless, static pushover analysis is not capable of capturing cumulative damage mechanisms, e.g., ratcheting and low cycle fatigue, due to its static nature. While the dynamic shakedown method is free of the aforementioned issues and is highly efficient, it is limited to simple constitutive material laws and is not capable of providing response time histories. Reduced order modeling is, on the other hand, a powerful approach that can, however, be limited in terms of potential speedup due to the need to solve a system that, although reduced, is still nonlinear. Recently, Li et al. [22, 23] extended the dynamic shakedown method to enable the estimation of response time histories while maintaining a computational speedup, compared to direct integration, of around an order of magnitude. However, due to the need to evaluate probabilistic metrics for describing performance, and therefore the need to evaluate thousands of nonlinear time histories, the aforementioned speedups are not adequate for general probabilistic performance assessments. An approach that has the potential to offer far greater speedups is that associated with the machine learning-based metamodeling of dynamic systems.

Typical metamodeling techniques centered on creating efficient function mappings, using,

for example, polynomials, neural networks, and Kriging, between the parameters characterizing uncertainty in both structure and excitation and a set of response metrics, for example, peak values or their statistics. These methods, however, only reconstruct a few response metrics and are not capable of providing estimates of response time histories which can be essential for the evaluation of coupled damage mechanisms or damage accumulation [7]. In response to this limitation, autoregressive models have been proposed for defining metamodels of the response trajectories of nonlinear dynamic systems [24, 25, 26]. More recently, through the aid of model order reduction, this method was extended for the estimation of the response trajectories of full-scale nonlinear structural systems [27, 28]. Alternatively, metamodeling techniques based on deep learning have been proposed [29, 30, 31] and successfully applied for the response estimation of wind excited structures [32, 33]. To facilitate application to high-dimensional systems and avoid the need to train individual metamodels for each response trajectory of interest, deep learning has been combined with model order reduction and shown to provide superior performance compared to traditional autoregressive models in estimating seismic responses [34]. Despite the progress in response time history metamodeling, this technique has not been systematically applied for the estimation of nonlinear dynamic response trajectories of wind-excited structural systems subject to general stochastic wind excitation.

This research is aimed at bridging this gap by introducing a deep learning-based response time history metamodeling framework that is capable of rapidly predicting the long-duration dynamic response trajectories at all degrees of freedom of nonlinear wind excited structural systems subject to general stochastic excitation modeling wind loading from various wind directions. The approach is illustrated within the context of probabilistic performance assessment with a focus on the massive speedups that can be achieved in evaluating the nonlinear dynamic response of the system.

### 2. Problem Definition and Underlying Models

### 2.1. Preamble

This work is focused on developing methods for rapidly characterizing the uncertainty in the nonlinear dynamic response of systems caused by wind directionality and the inherent record-to-record variability of wind load histories calibrated to wind speeds with target mean return intervals (MRIs). This is a key problem in probabilistic wind assessments [10], and requires a significant computational budget due to the numerical effort associated with propagating uncertainty through nonlinear dynamic systems driven by stochastic excitation with a duration of at least 1-hour (standard length for a wind load history used in PBWE [10]). This work seeks to provide methods to overcome this key hurdle by leveraging metamodeling based on deep learning. Using seismic engineering terminology, i.e., [35], while assuming wind speed as an "intensity measure", as is common in PBWE [10], this type of analysis can be termed an "intensity-based" performance assessment as the results are conditional on a specified value of the wind speed. The capability to perform intensity-based assessments can be used to directly infer performance over all wind intensities by carrying out a limited suite of intensity-based assessments with subsequent convolution, through the total probability theorem, with the "hazard curve" (defined in PBWE as the complementary cumulative distribution function of the maximum mean hourly wind speed). Therefore, the capability to carry out intensity-based assessments is key.

# 2.2. Intensity-based performance assessment and the sector-by-sector approach

Performance evaluation is generally formulated as a probabilistic problem associated with evaluating the failure probabilities, at the component or system level, against several predefined limit states. In wind engineering, both the aerodynamics of the building as well as the target wind speed vary considerably with direction. Many approaches have been developed to capture the effects of wind direction, e.g., the upper bound method, the sector-by-sector approach, the up-crossing method, and the storm passage method [36, 37]. Among these, the sector-by-sector approach is popular due to its simplicity and has been adopted in several PBWE frameworks [e.g. 38] as it does not require any assumptions on the response behavior of the system, i.e., linear and nonlinear systems are equally treatable. In the sector-by-sector approach, the space of wind direction is divided into  $N_{\text{sec}}$  exhaustive and non-overlapping sets, i.e., the sectors  $\mathbf{S}_k = [\alpha_{L,k}, \alpha_{U,k}]$  for  $k = 1, 2, ..., N_{\text{sec}}$  where  $\alpha_{L,k}$  and  $\alpha_{U,k}$  are the upper and lower bound of wind direction,  $\alpha$ , for sector k. The intensity-based performance of the

system can then be evaluated as:

$$P_{f|v_H} = \max_{k} \left[ P_{f|\mathbf{S}_k, v_{H,k}} \right] \tag{1}$$

where  $P_{f|v_H}$  is the failure probability conditional on the non-directional wind speed  $v_H$  of target return period while  $P_{f|\mathbf{S}_k,v_{H,k}}$  is the failure probability conditional on sector k and the sectorial wind speed,  $v_{H,k}$ , associated with target non-directional wind speed,  $v_H$ . Consistently with prevailing approaches, e.g., [5, 6, 13, 10, 38], the sector-by-sector approach is based on a worst case scenario model under the assumption of a constant wind direction during each windstorm. This approach is also adopted in the Prestandard for Performance-based Wind Design [10] for modeling wind direction during the inelastic assessment of the structural system. Nevertheless, it should be observed that the sector-by-sector approach does not contemplate multiple events over the lifespan of the structure nor does it consider wind direction change during a windstorm. From Eq. (1), it can be seen that in the sector-by-sector based approach,  $P_{f|v_H}$  is evaluated as the maximum conditional sectorial failure probability. Key to the sector-by-sector approach is therefore the estimation of  $P_{f|\mathbf{S}_k,v_{H,k}}$  that can be written in the following general form:

$$P_{f|\mathbf{S}_k, v_{H,k}} = \int \dots \int_{g(\mathbf{y}, \alpha, v_{H,k}) \le 0} f(\mathbf{Y}|\alpha, v_{H,k}) d\mathbf{y} |dH(\alpha|\mathbf{S}_k, v_{H,k})|$$
(2)

where:  $\mathbf{Y}$  is the high-dimensional vector collecting the random variables modeling the stochasticity (record-to-record variability) of the external dynamic wind loads;  $f(\mathbf{Y}|\alpha)$  is the probability density function of  $\mathbf{Y}$  conditioned on  $\alpha$  and  $v_{H,k}$ ;  $H(\alpha|\mathbf{S}_k)$  is the complementary cumulative distribution function (CCDF) of  $\alpha$  conditioned on  $\mathbf{S}_k$  and  $v_{H,k}$ ;  $g(\mathbf{y})$  denotes a limit state function of interest with  $g(\mathbf{y}) \leq 0$  indicating failure, e.g., interstory drift exceeding a predefined limit. The evaluation of Eq. (2) is often carried out using stochastic simulation schemes, e.g., stratified sampling [39, 40], and therefore generally requires the repeated evaluation of the long-duration nonlinear dynamic response of the system therefore creating a significant computational bottleneck.

#### 2.3. Structural and wind load model

## 2.3.1. Nonlinear structural model

The nonlinear dynamic response of a wind-excited structural system can be estimated by solving the following equations of motion:

$$\mathbf{M\ddot{u}}(t) + \mathbf{C\dot{u}}(t) + \mathbf{F}_{nl}(t) = \mathbf{F}(t; \alpha, v_H, \mathbf{y})$$
(3)

where  $\mathbf{M}$  and  $\mathbf{C}$  are respectively the  $N \times N$  structural mass and damping matrices with N the total number of degrees of freedom (DOFs) of the system;  $\mathbf{u}(t)$ ,  $\dot{\mathbf{u}}(t)$  and  $\ddot{\mathbf{u}}(t)$  are the  $N \times 1$  displacement, velocity, and acceleration response vectors respectively;  $\mathbf{F}_{nl}(t)$  is the  $N \times 1$  nonlinear restoring force vector;  $\mathbf{F}(t; \alpha, v_H, \mathbf{y})$  is a realization of the  $N \times 1$  stochastic wind excitation vector defined for the wind direction,  $\alpha$ , and wind speed,  $v_H$ , as well as  $\mathbf{y}$ , a realization of  $\mathbf{Y}$ .

### 2.3.2. Stochastic wind load model

Given  $\alpha$  and  $v_H$ , various models can be adopted for representing  $\mathbf{F}(t; \alpha, v_H, \mathbf{y})$ . In this work, the data-driven spectral proper orthogonal decomposition model outlined in Duarte et al. [41] is adopted as it enables the direct capture of the complex aerodynamics seen in the wind tunnel, e.g., vortex shedding and detached flow, in the stochastic wind loads. This model is based on representing the *i*th component of  $\mathbf{F}(t; \alpha, v_H, \mathbf{y})$  in the following form [42, 41]:

$$F_{i}(t; v_{H}, \alpha, \mathbf{y}) = \sum_{l_{\Upsilon}=1}^{N_{\Upsilon}} \sum_{k_{\omega}=1}^{N_{\omega}-1} 2|\Upsilon_{il_{\Upsilon}}(\omega_{k_{\omega}}; \alpha)| \sqrt{\chi_{l_{\Upsilon}}(\omega_{k_{\omega}}; v_{H}, \alpha)\Delta\omega} \cos(\omega_{k_{\omega}} t + \vartheta_{il_{\Upsilon}}(\omega_{k_{\omega}}; \alpha) + Y_{l_{\Upsilon}k_{\omega}})$$

$$\tag{4}$$

where:  $\Upsilon_{il_{\Upsilon}}(\omega_{k_{\omega}};\alpha)$  is the *i*th component of the  $l_{\Upsilon}$ th eigenvector at frequency  $\omega_{k_{\omega}}$  with  $\chi_{l_{\Upsilon}}(\omega_{k_{\omega}};\bar{v}_{H},\alpha)$  the corresponding eigenvalue;  $N_{\Upsilon}$  is the number of spectral modes considered in the representation;  $N_{\omega}$  is the total number of discrete frequency steps of the decomposition;  $\vartheta_{il_{\Upsilon}}(\omega_{k_{\omega}};\alpha)$  is a complex angle that can be written in the following form  $\vartheta_{il_{\Upsilon}}(\omega_{k_{\omega}};\alpha) = \frac{\operatorname{Imag}(\Upsilon_{il_{\Upsilon}}(\omega_{k_{\omega}};\alpha))}{\operatorname{Real}(\Upsilon_{il_{\Upsilon}}(\omega_{k_{\omega}};\alpha))}$ ; while  $Y_{l_{\Upsilon}k_{\omega}}$  is a random phase angle uniformly distributed in  $[0,2\pi)$  and constituting a component of  $\mathbf{Y}$  modeling the stochasticity of  $\mathbf{F}(t)$ . To ensure reasonable initial and final conditions,  $\mathbf{F}(t)$  is generally multiplied by an appropriate envelope function, e(t). A common choice for defining e(t) is to consider a linear ramp over the first few minutes of F(t) and a linear ramp over the last few minutes of  $\mathbf{F}(t)$  [19, 38].

# 2.4. Discussion and challenges

Solving Eq. (3) is usually not a trivial task, especially in the case of complex and highdimensional nonlinear systems. Moreover, the excitation associated with extreme wind events has durations in the order of hours further exacerbating computational demand. This computational challenge is compounded if stochastic simulation schemes are used for propagating uncertainty through the models in estimating Eq. (2). This research aims to alleviate this issue through implementing deep learning metamodeling techniques, the theory of which will be outlined in the next section.

## 3. The LSTM-based metamodeling framework

## 3.1. Preamble

This section introduces the metamodeling approach underpinning the framework of this work. The approach is based on first using a data-driven model order reduction scheme by leveraging proper orthogonal decomposition (POD) over a set of response samples estimated through solving from Eq. (3). Subsequently, the reduced space is learned by a LSTM neural network which, once trained, is capable of reproducing the time response of the nonlinear system for a given wind speed and direction with negligible computational effort.

#### 3.2. Model order reduction

In general, structural systems of practical interest have many thousands of DOFs that feed into the limit state functions, g, of Eq. (2) in determining the performance of the system. However, learning such high-dimensional systems can be extremely complex. To overcome this difficulty, a Galerkin model order reduction is considered before attempting to learn the dynamics of the system. A coordinate transformation matrix,  $\phi$ , is therefore used to reduce Eq. (3) to the form:

$$\mathbf{m}\ddot{\mathbf{q}}(t) + \mathbf{c}\dot{\mathbf{q}}(t) + \mathbf{f}_{nl}(t) = \mathbf{p}(t; \mathbf{y}, \alpha, v_H)$$
(5)

where:  $\mathbf{m} = \boldsymbol{\phi}^{\mathrm{T}} \mathbf{M} \boldsymbol{\phi}$  and  $\mathbf{c} = \boldsymbol{\phi}^{\mathrm{T}} \mathbf{C} \boldsymbol{\phi}$  are the reduced mass and damping matrices, respectively;  $\mathbf{q}(t)$ ,  $\dot{\mathbf{q}}(t)$ , and  $\ddot{\mathbf{q}}(t)$  are the displacement, velocity, and acceleration vectors in the reduced space; while  $\mathbf{f}_{\mathrm{nl}}(t) = \boldsymbol{\phi}^{\mathrm{T}} \mathbf{F}_{\mathrm{nl}}(t)$  and  $\mathbf{p}(t; \mathbf{Y}, \alpha, v_H) = \boldsymbol{\phi}^{\mathrm{T}} \mathbf{F}(t; \mathbf{Y}, \alpha, v_H)$  are respectively the reduced nonlinear restoring force vector and excitation force vector. In particular, an appropriately constructed transformation,  $\boldsymbol{\phi}$ , ensures an accurate approximation of  $\mathbf{u}(t) \approx \boldsymbol{\phi} \mathbf{q}(t)$  can be achieved from only a few reduced coordinates. An effective approach for estimating the coordinate transformation,  $\boldsymbol{\phi}$ , is to apply POD on a response matrix,  $\mathbf{U}$ , defined by

collecting a series of response snapshots of the system estimated by solving Eq. (3) for a limited set of excitation samples. In particular, POD is generally implemented by applying the singular value decomposition:

$$\mathbf{U} = \mathbf{\Phi} \mathbf{\Lambda} \mathbf{\Psi}^{\mathrm{T}} \tag{6}$$

where  $\Phi$  and  $\Psi$  are unitary matrices collecting respectively the left and right singular vectors;  $\Lambda$  is a pseudo diagonal matrix with the diagonal entries,  $\Lambda(i,i)$ , the *i*th largest singular value  $\lambda_i$ . In particular,  $\lambda_i^2$  indicates the energy of  $\mathbf{U}$  projected onto the *i*th left singular vector. To define  $\phi$ , it is, therefore, reasonable to keep the first m significant left singular vectors, which define a subspace that captures the majority of the energy in the structural response.

Through this process, the original N-dimensional problem of Eq. (3) is reduced to the m-dimensional system of Eq. (5) where in general  $m \ll N$ . Despite the significantly reduced size of the problem, the evaluation of  $\mathbf{f}_{\rm nl}(t)$  at each time step generally requires evaluating the high-dimensional model therefore limiting the computational advantage of Eq. (5). The idea on which the framework of this work is based is to learn the dynamic input and output relationship of the reduced space, i.e., the relationship between  $\mathbf{p}(t)$  and  $\mathbf{q}(t)$  through the use of LSTM deep neural networks.

## 3.3. LSTM configurations

Typically an LSTM neural network consists of one or more LSTM layers, that can be used to learn the dynamics of a time series, and a fully connected layer for transferring the hidden states into outputs of correct dimension. In particular, the LSTM layer can be mathematically described as follows:

$$\mathbf{g}_{f}(\tau) = \sigma_{g}(\boldsymbol{\theta}_{fH}^{T}\mathbf{y}(\tau - 1) + \boldsymbol{\theta}_{fI}^{T}\mathbf{x}(\tau) + \mathbf{b}_{f})$$
(7)

$$\mathbf{g}_{i}(\tau) = \sigma_{g}(\boldsymbol{\theta}_{i,H}^{T}\mathbf{y}(\tau - 1) + \boldsymbol{\theta}_{i,I}^{T}\mathbf{x}(\tau) + \mathbf{b}_{i})$$
(8)

$$\mathbf{g}_{o}(\tau) = \sigma_{g}(\boldsymbol{\theta}_{o,H}^{T}\mathbf{y}(\tau - 1) + \boldsymbol{\theta}_{o,I}^{T}\mathbf{x}(\tau) + \mathbf{b}_{o})$$
(9)

$$\Delta \mathbf{C}(\tau) = \sigma_{s}(\boldsymbol{\theta}_{c,H}^{T}\mathbf{y}(\tau - 1) + \boldsymbol{\theta}_{c,I}^{T}\mathbf{x}(\tau) + \mathbf{b}_{c})$$
(10)

$$\mathbf{C}(\tau) = \mathbf{g}_{\mathbf{f}}(\tau) \circ \mathbf{C}(\tau - 1) + \mathbf{g}_{\mathbf{i}}(\tau) \circ \Delta \mathbf{C}(\tau)$$
(11)

$$\mathbf{y}(\tau) = \mathbf{g}_{o}(\tau) \circ \sigma_{s}(\mathbf{C}(\tau)) \tag{12}$$

where  $\mathbf{x}$  and  $\mathbf{y}$  are respectively the input and output series of the LSTM layer;  $\tau$  denotes the time step of the input/output sequence;  $\mathbf{g}_{\mathrm{f}}(\tau)$ ,  $\mathbf{g}_{\mathrm{i}}(\tau)$ , and  $\mathbf{g}_{\mathrm{o}}(\tau)$  are the forget, input, and output gates, respectively;  $\mathbf{C}(\tau)$  is the current cell state with  $\mathbf{C}(\tau-1)$  the previous cell state;  $\Delta \mathbf{C}(\tau)$  is the new information on the cell state;  $\sigma_{\mathrm{g}}(\cdot)$  and  $\sigma_{\mathrm{o}}(\cdot)$  are respectively the gate and state activation functions (typically sigmoid and/or hyperbolic tangent functions);  $\circ$  is the Hadamard (element-wise) product operator; while  $\boldsymbol{\theta}_{\mathrm{f,H}}$ ,  $\boldsymbol{\theta}_{\mathrm{i,H}}$ ,  $\boldsymbol{\theta}_{\mathrm{o,H}}$ ,  $\boldsymbol{\theta}_{\mathrm{f,I}}$ ,  $\boldsymbol{\theta}_{\mathrm{i,I}}$ ,  $\boldsymbol{\theta}_{\mathrm{o,I}}$ ,  $\boldsymbol{\theta}_{\mathrm{c,I}}$ ,  $\boldsymbol{b}_{\mathrm{f}}$ ,  $\mathbf{b}_{\mathrm{i}}$ ,  $\mathbf{b}_{\mathrm{o}}$ , and  $\mathbf{b}_{\mathrm{c}}$  are the tunable parameters of the LSTM network that are to be calibrated during training and are collected in the vector  $\boldsymbol{\theta}$  in the following. The fundamental property of an LSTM architecture that makes it suitable for learning the long time sequences of this work can be traced back to how the cell state flows through the network using only linear operations. This ensures straightforward back-propagation of gradient information therefore helping avoid gradient vanishing and exploding problems.

The length of the input and output series,  $\mathbf{p}(t)$  and  $\mathbf{q}(t)$ , in wind engineering can be significant therefore hindering the training of the LSTM and operation in simulation mode once trained. To overcome this,  $\mathbf{p}(t)$  and  $\mathbf{q}(t)$  can be approximated through the wavelet transformation and therefore represented in terms of much shorter sequences of wavelet coefficients  $\mathbf{W}_{s,\mathbf{p}}(\tau)$  and  $\mathbf{W}_{s,\mathbf{q}}(\tau)$  [43, 32, 34]. Within this context, the LSTM neural network takes  $\mathbf{W}_{s,\mathbf{p}}(\tau)$  as input and predicts  $\mathbf{W}_{s,\mathbf{q}}(\tau)$ , while the training of the LSTM can be formulated as:

$$\boldsymbol{\theta}^* = \arg\min_{\boldsymbol{\theta}} \mathcal{L}(\boldsymbol{\theta}) \tag{13}$$

where  $\theta^*$  is the optimal parameter vector and  $\mathcal{L}(\theta)$  is the following loss function describing the goodness of fit:

$$\mathcal{L}(\boldsymbol{\theta}) = \frac{1}{2} \mathbb{E}_{\tau} \left[ \sum_{j} (W_{s,q_j}(\tau) - W_{\boldsymbol{\theta},s,q_j}(\tau))^2 \right]$$
 (14)

where  $\mathbb{E}_{\tau}$  is the operator of the expectation over  $\tau$  while  $W_{\theta,s,q_j}(\tau)$  is the predicted output for the jth reduced coordinate from the LSTM neural network with parameters  $\theta$ .

Eq. (13) can be efficiently solved by gradient-based algorithms by targeting the predicted outputs of a set of ground truth data. The parameters  $\theta$  are tuned through an iterative step-by-step process until the discrepancy between the predicted outputs and the ground truth data is reduced to a satisfying level. Once trained, and given a new wind excitation, the

LSTM neural network can be used to predict the wavelet coefficients of the reduced outputs from which the response of the system at all DOFs can be directly estimated by applying the inverse wavelet and coordinate transformations. It should be noted that the LSTM neural network requires neither computation in the full space nor iterations. In addition, the evaluation of neural networks can easily be performed using Graphics Processing Units (GPUs). This leads to massive speedups in predicting response time histories of nonlinear systems once the LSTM is trained.

## 4. The Training and Simulation Scheme

## 4.1. Preamble

The LSTM metamodel of Sec. 3 potentially represents a powerful response simulator for dramatically speeding up the assessment of Eq. (1) by facilitating the stochastic simulation-based assessment of  $P_{f|\mathbf{S}_k,v_{H,k}}$ . However, the following two major challenges exist:

- 1. Wind excitation in different wind directions can vary significantly. For example, the mean component of wind excitation varies from zero for acrosswind type loading to a considerable portion of the overall load for alongwind type loading. As a result, the mechanisms related to the accumulation of inelastic deformation can vary significantly. Indeed, wind excitation with an important mean component can lead to a ratcheting-type failure mechanism while zero-mean wind excitation can lead to low cycle fatigue failure. This variation in loading and subsequent response complicates the training of the LSTM metamodel as it must be capable of capturing the intricacies of the responses for not only alongwind/acrosswind type loading, but also loading from all other wind directions.
- 2. Unlike typical seismic records that have durations in the order of minutes, wind excitation typically has durations in the order of hours leading to long response time histories. Ensuring an adequate time step for capturing the high-frequency content of the response (e.g., less than 0.5 seconds), can lead to time sequences of excessive length (even after wavelet transformation) that can cause significant memory issues during training due to the need for back-propagation. This is especially true if GPUs are used as they typically have limited memory capacity.

The possibility of training a single LSTM metamodel capable of addressing the points outlined above has not been explored up to date. The next section will outline a training scheme to this end.

# 4.2. Training

To address the first challenge outlined in Sec. 4.1, it is proposed to train the LSTM network considering a set of data that contains an equal number,  $N_{\alpha}$ , of randomly generated samples for each discrete wind direction,  $\alpha_i$ , considered in modeling the aerodynamic response of the system. Generally,  $N_d$  wind directions are considered for characterizing the aerodynamic response of the system resulting in  $\alpha_i$  varying between  $i=1,...,N_d$ . It should be noted that, because of aspects such as symmetry in loading, the wind directions used in training do not necessarily represent an equidistant discretization of wind direction as this would lead to duplicate training data. Each sample is generated considering the non-directional wind speed,  $v_H$ , as the sectorial wind speeds satisfy the condition  $v_{H,k} \leq v_H$  (i.e., by considering  $v_H$ , the network will be trained on data presenting an upper bound on wind intensity). By following this scheme, a total of  $N_T = N_{\alpha} \times N_d$  samples are used to train the LSTM network within the reduced space. Because an equal number of samples are considered for each unique wind direction during training, the LSTM experiences the type of response variability expected due to the variability in wind direction and therefore should be capable of predicting the expected variability in nonlinear responses.

To address the second challenge, it is proposed to train the LSTM network using response samples of reduced duration,  $t_s$ , as compared to the simulation horizon, T, i.e., the duration of the stochastic wind loads  $\mathbf{F}(t)$ . The reasoning underpinning this idea can be traced back to how wind excitation is generally modeled as stationary. Therefore, for a given wind speed and direction, it is hypothesized that the damage accumulation experienced by the system in  $[0, t_s]$  will be similar to that experienced in  $(t_s, T]$  therefore allowing the LSTM network to sufficiently learn the system from a total of  $N_T$  truncated response samples.

## 4.3. Simulation strategy

Once trained, the LSTM metamodel can be used to directly estimate the sectorial failure probabilities,  $P_{f|\mathbf{S}_k,v_{H,k}}$  for  $k=1,2,...,N_{\text{sec}}$ , using direct Monte Carlo simulation and therefore

as:

$$P_{f|\mathbf{S}_k,v_{H,k}} = P(g \le 0|\mathbf{S}_k,v_{H,k}) \approx \sum_{i=1}^{N_{\text{mc}}} \kappa(0;g_i|\mathbf{S}_k,v_{H,k})$$
(15)

where  $\kappa(\cdot; g_k | \mathbf{S}_k, v_{H,k})$  is a kernel function constructed from the response samples of the limit state function  $g_k$  evaluated using the trained LSTM metamodel for wind directions in  $\mathbf{S}_k$  and a wind speed of  $v_{H,k}$ , while  $N_{\text{mc}}$  is the total number of samples used in the Monte Carlo simulation.

The massive computational speedups generally enjoyed by LSTM metamodels (in the order of magnitudes) make the evaluation of Eq. (15) a trivial computational task even for large values of  $N_{\rm mc}$  and therefore Monte Carlo samples. It should also be observed that the estimator of Eq. (15) can be used to directly estimate probability distributions, such as the CCDF, by simply replacing g with the response of interest and evaluating Eq. (15) for a suite of threshold values.

The proposed deep learning-based framework for estimating  $P_{f|v_H}$ , including the training phase, is summarized in Fig. 1.

## 5. Case Study

The proposed framework is illustrated through application to a 37-story steel moment-resisting frame subject to stochastic wind excitation. In particular, the building is assumed to be located in New York City and has a first story height of 6 m with all subsequent floors having a height of 4 m leading to a total height of 150 m. The frame considered in this study is one of the six identical X-direction moment resisting frames, as indicated in Fig. 2. The frame has square box sections as columns and standard W24 wide flange sections as beams. The variation of section size over the height of the building is summarized in Table 1. Both the columns and beams are considered to be manufactured from Grade 50 steel. In addition, the structural mass is calculated as the sum of the structural self-weight and a carried mass of 100 kg/m<sup>3</sup> considered acting over the influence area of the frame. Because the frame is considered as part of a 3D building, the wind loading, taken as 1/6 of the total X-direction loading, can be estimated for all wind directions.

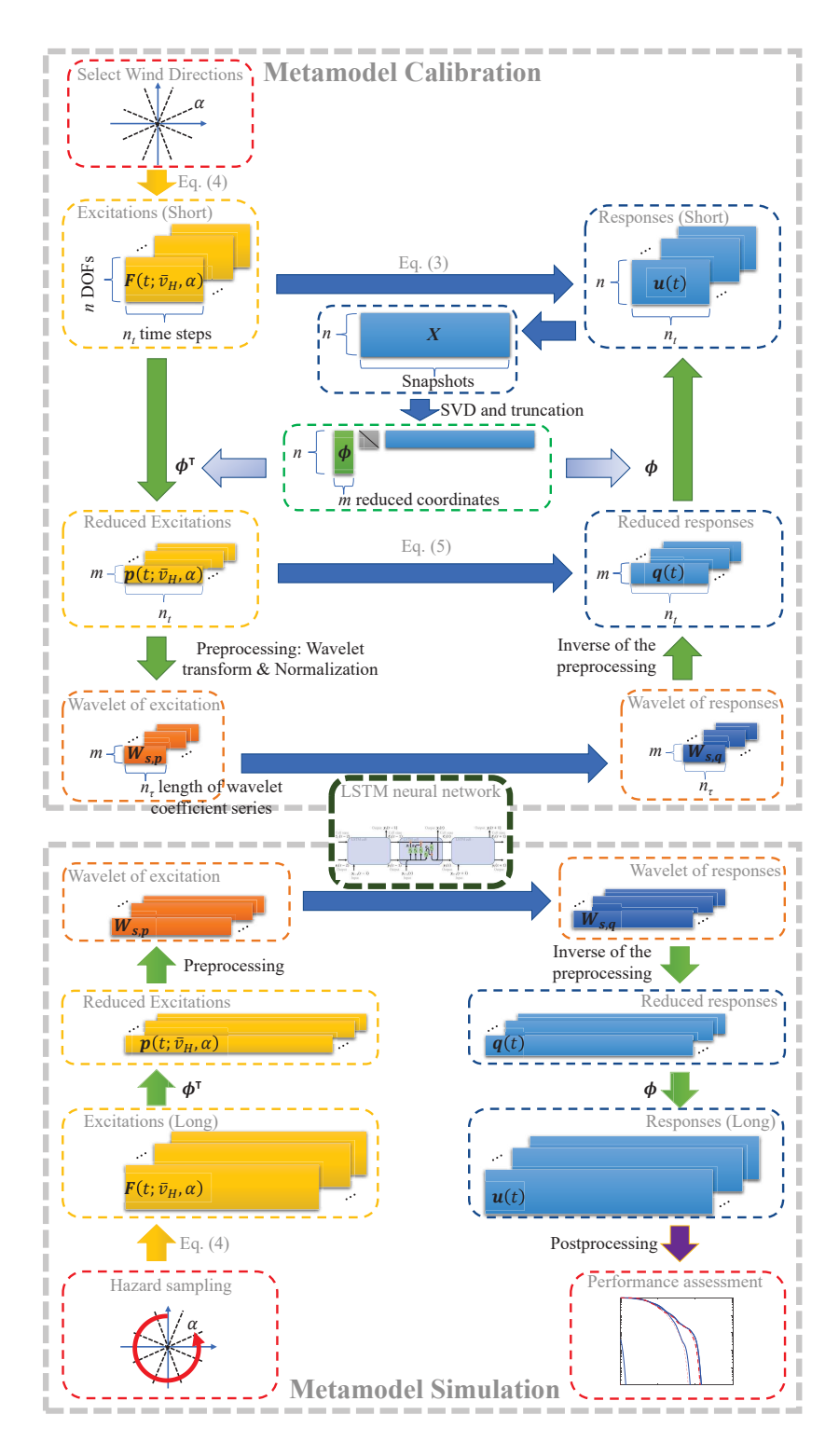


Figure 1: Schematic of the proposed deep learning-based metamodeling framework for rapid intensity-based probabilistic wind performance assessment.

Table 1: Section sizes of the steel frame.

	Wide	e-flange Beams	Box Columns			
Level	Section size	Plastic modulus (m <sup>3</sup> )	Section size (m)	Plastic modulus $(m^3)$		
1-10	$W24 \times 192$	0.0092	D = 0.5	0.0094		
11-20	$W24\times192$	0.0092	D = 0.5	0.0094		
21-30	$W24 \times 103$	0.0046	D = 0.4	0.0048		
31-37	$W24\times103$	0.0046	D = 0.35	0.0032		

# 5.1. High-fidelity model

The structure is modeled in the finite element environment OpenSees (Open System for Earthquake Engineering Simulation) [44]. Fiber-based displacement-based elements with a 5-point Gauss-Legendre integration scheme are adopted for modeling the frame. Distributed plasticity is therefore considered. For the steel fibers, an elastic perfectly plastic constitutive law is adopted, with Young's modulus of 200 GPa and the yield strength of 355 MPa. In addition, a rigid diaphragm constraint is enforced and the structural mass is lumped at the

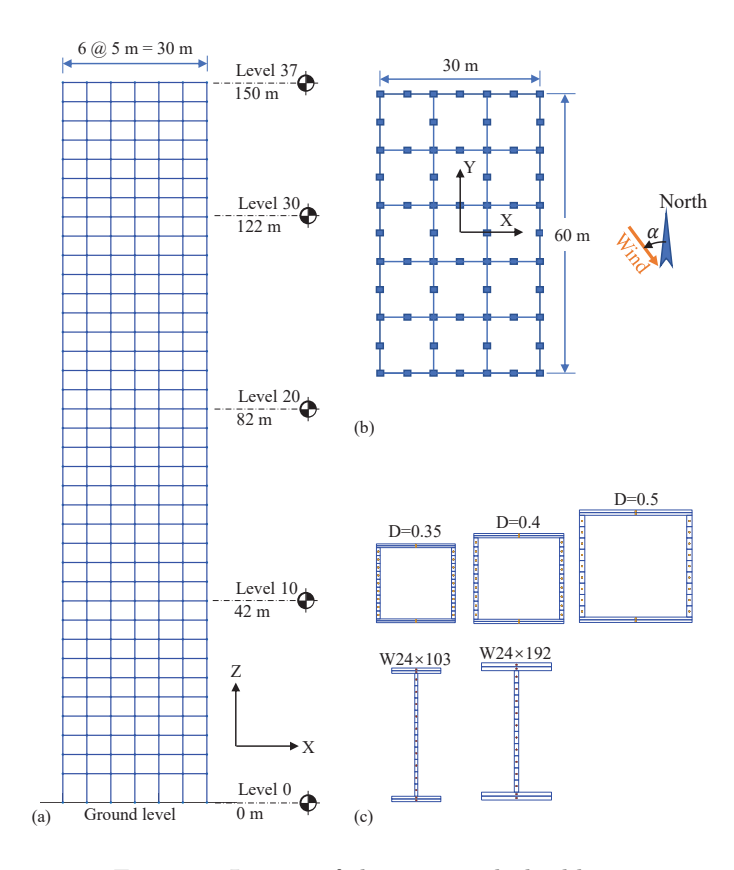


Figure 2: Layout of the case study building.

master node of each floor. The first two natural frequencies are respectively 0.19 Hz and 0.53 Hz. A Rayleigh damping model is adopted, with the damping ratio fixed at 2.5% for the first two natural frequencies.

## 5.2. Wind load

For this case study, the wind directions are separated into 8 equally sized sectors, as illustrated in Fig. 3. In particular, as adopted in Chuang and Spence [38], the sectorial wind speeds are linearly related to their non-directional counterparts through the relationship  $v_{H,k} = K_k v_H$  where  $K_k$  are site-specific wind directionality factors. The  $K_k$  values used in this study are those found in Chuang and Spence [38] and reported in Table 2. It should be observed that because the  $K_k$  values are identified from the relationship:  $v_{H,k}/v_H = K_k$  with  $v_{H,k}$  estimated by fitting a wind speed distributions to directional sector specific wind data, the directionality factors explicitly account for any phenomenological wind climate effects, e.g., likelihood of windstorms occurring in a particular sector. The non-directional mean hourly wind speed,  $v_H$ , at which the performance assessment was carried out was 56.48 m/s for a stationary time horizon of T = 3600 s. This was estimated from the ASCE 7-22 [45] hazard maps for exposure B and corresponded to a mean recurrence interval (MRI) of 10000 years. Considering how the building was designed to be predominately elastic for a wind loading corresponding to a wind speed with 1700 MRI (risk category II structure [45]), this level of wind loading is expected to cause a noticeable inelastic response.

The stochastic wind load model of Eq. (4) was calibrated to wind tunnel data collected on a 1/300 scaled rigid model of the building and part of the Tokyo Polytechnic University's (TPU) aerodynamic database [46]. The data was measured using 512 synchronously measured pressure taps at a sampling frequency of 1000 Hz and a mean wind speed at the model top of 11 m/s. The measured data was further processed to estimate two time-varying translational floor loads acting in the X and Y directions and a torsional moment around the vertical Z direction. This raw data was scaled by matching the reduced frequency at the model and full scale. Spectral interpolation was then used to ensure all wind load samples generated from Eq. (4) had a cutoff frequency of 1 Hz, i.e., a sampling frequency of 0.5 Hz. It is noted that the wind tunnel test data was only available for  $\alpha = 0^{\circ}$ ,  $10^{\circ}$ , ...,  $90^{\circ}$ . Symmetry was therefore used to extend the data to all 36 wind directions,  $\alpha = 0^{\circ}$ ,  $10^{\circ}$ , ...,  $360^{\circ}$ , as

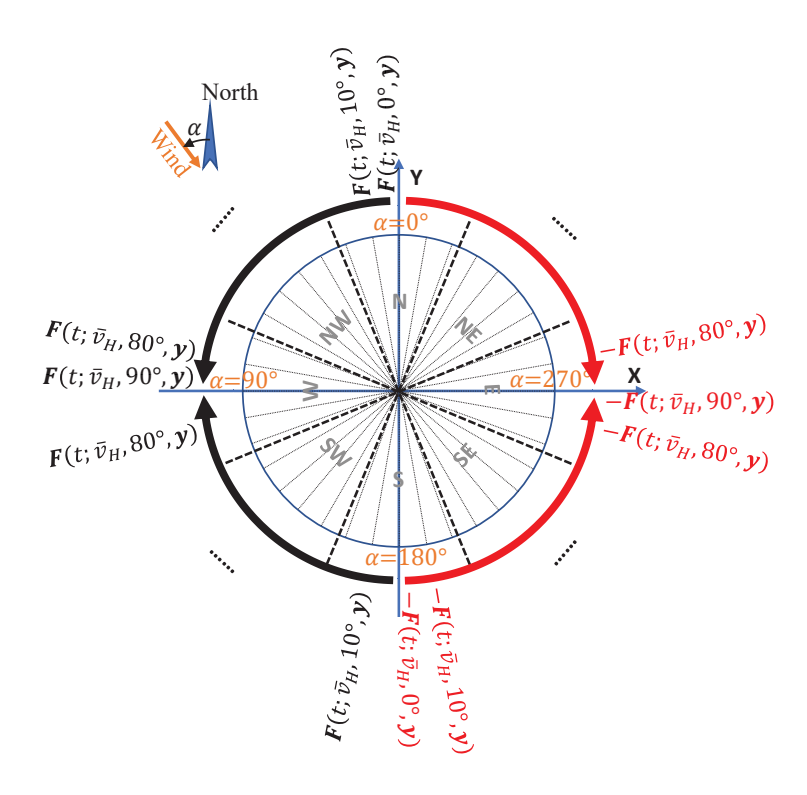


Figure 3: Illustration of how symmetry was used to assign  $\mathbf{F}(t; \bar{v}_H, \alpha, \mathbf{y})$  for  $\alpha \in \{100^\circ, 110^\circ, ..., 360^\circ\}$  from the knowledge of  $\mathbf{F}(t; \bar{v}_H, \alpha, \mathbf{y})$  for  $\alpha \in \{0^\circ, 10^\circ, ..., 90^\circ\}$ . Red arrows indicate when a change of sign was also needed.

Table 2: Directionality factors of the wind sectors.

Sector	N	Е	S	W	NE	SE	SW	NW
$K_k$	0.88	0.88	0.84	0.84	0.84	0.88	1.00	0.92

illustrated in Fig. 3.

### 5.3. Configuration and training of the LSTM metamodel

### 5.3.1. Training Data

As outlined in Sec. 5.2, wind tunnel data is available in ten-degree increments, i.e.,  $\Delta \alpha = 10^{\circ}$ . Due to the symmetry of the problem, unique loading conditions are experienced by the structure only for the following  $N_d = 19$  wind directions  $\{0^{\circ}, ..., 90^{\circ}, 270^{\circ}, ..., 350^{\circ}\}$ . Training was therefore carried out for this set of wind directions. In particular,  $N_{\alpha} = 43$  was considered leading to a total of  $N_T = N_{\alpha} \times N_d = 817$  training samples. A reduced duration (compared to the T = 3600 s stationary duration of the performance assessment) of  $t_s = 600$ 

s was considered in training (this included a 60 s initial and final load ramp and 60 s of appended zero loading for estimating the residual response). Consistently with ASCE 7-22 [45], the target mean hourly wind speed,  $v_H = 56.48$  m/s, was multiplied by 1.06 to ensure it represented the maximum 10-minute average wind speed. The high-fidelity response of the system was obtained by solving Eq. (3) by direct integration using the adaptive solver outlined in Li and Spence [34] with a default time step of 0.02 s.

The singular vectors defining the reduced space were estimated from the calibration set using 1200 evenly spaced snapshots for each response sample. A threshold of  $\eta = 99.999\%$  for mode truncation was implemented, and a three-dimensional reduced space was seen to be sufficient for all wind directions. The reduced responses are estimated by solving Eq. (5) with a 4th order Runge-Kutta scheme by enforcing a relative error tolerance of  $10^{-5}$ .

## 5.3.2. LSTM configuration

The deep neural network considered in this work had an LSTM layer with 200 hidden units, a dropout layer with a dropout probability of 50% to alleviate potential overfitting issues, and a fully connected layer. Both the input and output dimensions are three, consistent with the dimensionality of the reduced system. For the LSTM training, both the reduced excitation and response in the calibration set are preprocessed by the wavelet transform with the 6th-order Daubechies function. Further, the preprocessed calibration set is randomly divided into a training set with 750 samples and a validation set of 67 samples. The adaptive moment estimation (Adam) algorithm with a constant learning rate of 0.005 is used to train the LSTM neural network. In every training iteration, a randomly selected mini-batch of 75 samples from the training set is used to calculate the gradient. Every 50 iterations, the loss value over the validation set is evaluated to monitor potential overfitting issues, and an early stop is triggered if unacceptably high overfitting is detected. The training is performed until a maximum epoch of 4000 is reached or the loss function ceases to show a decreasing trend. All the computations involved in this work were performed on a personal computer with Intel(R) Xeon(R) E-2236 CPU @3.40 GHz, NVIDIA Quadro RTX 4000 GPU, and 32 Gb RAM.

The loss associated with the training and validation set for the training process is shown

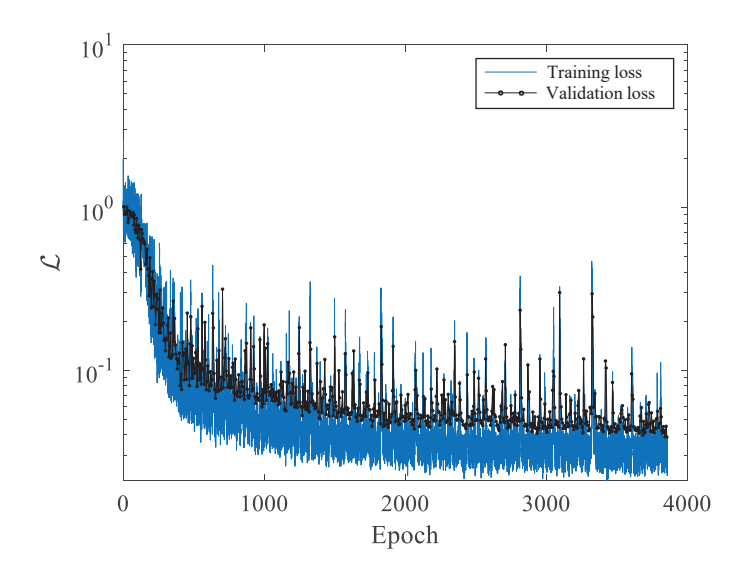


Figure 4: Loss curve for the training and validation data set.

in Fig. 4. It is seen that both the training and validation loss progressively decrease with the training epochs until convergence. The validation loss is slightly higher than the training loss but does not indicate a significant overfitting issue.

#### 5.3.3. Test data results

Five samples for each wind direction were considered for testing leading to a total of 180 test samples. Example displacement time histories at two locations and a wind direction of  $\alpha=270^\circ$  are shown in Fig. 5 together with the peak values over all wind directions estimated by the LSTM metamodel and the high-fidelity OpenSees model. In comparing the extreme values, a statistical peak was used defined by the mean plus one standard deviation (mean and standard deviation estimated from the response corresponding to the unramped stationary portion of loading). It is seen that, even in the presence of important nonlinearity (observable from the noticeable residual displacement at the end of the time histories), the LSTM metamodel was capable of reconstructing the entire response time history with remarkable accuracy. The comparison of the peak values shows how high accuracy holds over the entire test data set. In addition, Fig. 4 also shows how the LSTM metamodel is capable of accurately reproducing the fiber strain and stress response of the system, illustrated for a column fiber at the base of the structure in terms of example time histories, hysteretic curve, and peak values over all test data. Finally, the calibrated LSTM metamodel was seen to be

over 70000 times faster than the high-fidelity OpenSees model.

## 5.4. Intensity-based performance assessment by LSTM metamodel

## 5.4.1. Nonlinear time history prediction

As mentioned in Sec. 5.2, the stationary time horizon of interest to the performance assessment of this work is T = 3600 s (to which 3 minutes are added in terms of a linear initial and final ramp of 1-minute duration and a free vibration of 1 minute at the end to enable direct estimation of the residual response of the system). To verify the capability of the LSTM metamodel to predict responses over this time horizon notwithstanding how it was trained over a reduced time horizon of  $t_s = 600$  s, a set of 210 load histories was generated with stationary duration T = 3600 s. These samples were evenly distributed in the three critical sectors highlighted in Fig. 6 as, due to the symmetry of the problem and the directionality factors of Table 2, all other sectors will have responses strictly less than or equal to these sectors. Each sector was therefore assigned 70 randomly generated stochastic load histories with wind direction varying following a uniform probability mass function. Example displacement time histories estimated by the LSTM metamodel and the high-fidelity OpenSees model are shown in Fig. 7 for two locations and the South West sector together with the sample peak values over all the wind directions of the three critical sectors. It is seen that, even in the presence of important nonlinearity (observable from the noticeable residual displacement at the end of the time histories), the LSTM metamodel was capable of reconstructing over the entire time horizon the response time histories with remarkable accuracy. The comparison of the peak values shows how high accuracy holds for all three of the sectors. In addition, Fig. 7 also shows how the LSTM metamodel is capable of accurately reproducing the fiber strain and stress response of the system, illustrated for a column fiber at the base of the structure in terms of example time histories, hysteretic curve, and peak values estimated for all three of the sectors.

## 5.4.2. Probabilistic performance assessment

In this section, the LSTM metamodel is used to estimate the performance of the system through the sector-by-sector framework outlined in Sec. 2.2. In particular, leveraging how the critical sectors are North, South West, and East, the failure probabilities were estimated

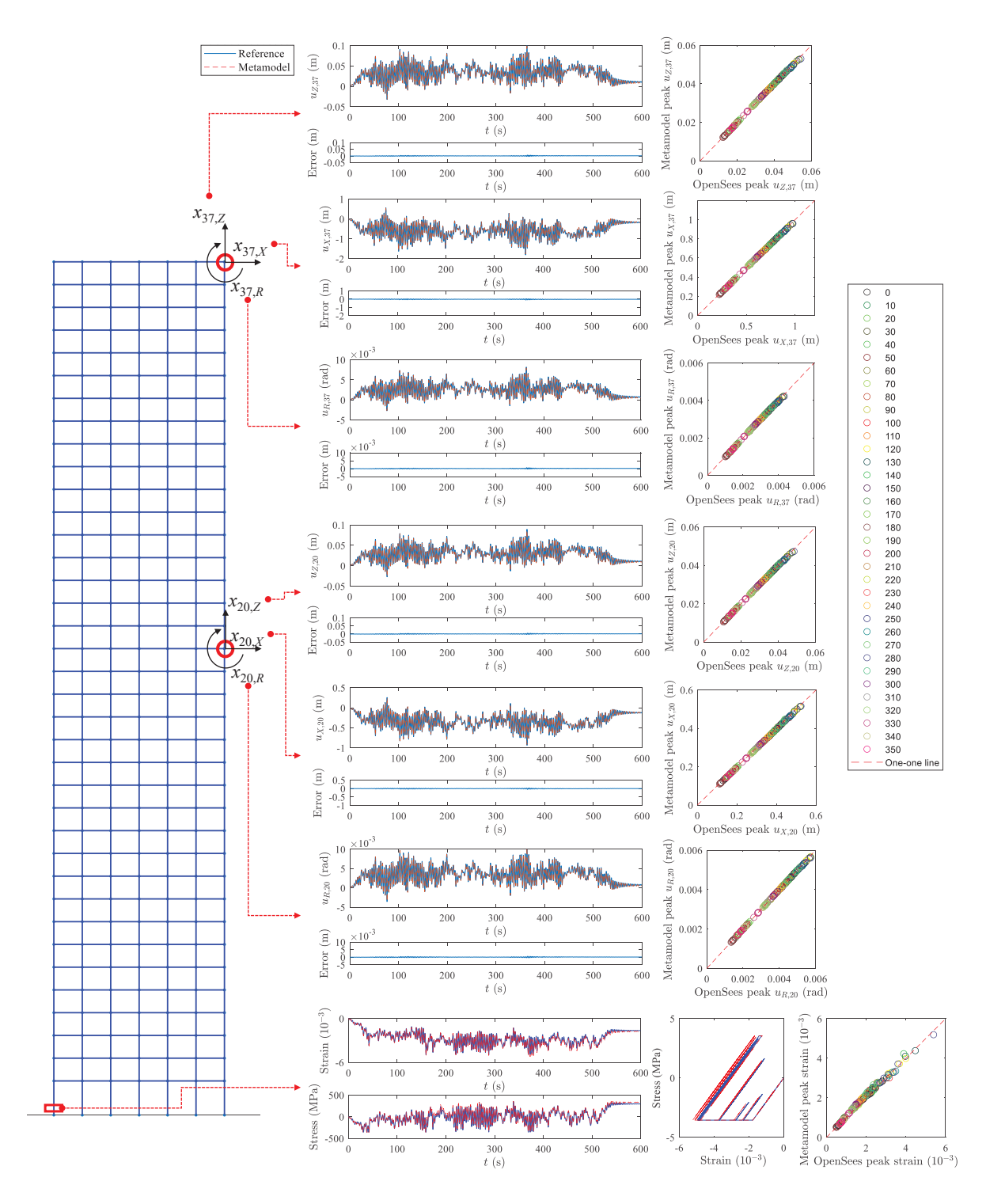


Figure 5: Test data performance of the trained LSTM metamodel. Example time histories for a wind direction of  $\alpha = 270^{\circ}$  and horizontal, vertical, and rotational responses at two locations of the structure as well as the stress and strain fiber response for a column at the base of the structure (corresponding hysteretic curve also shown). Peak values over all test data are also shown.

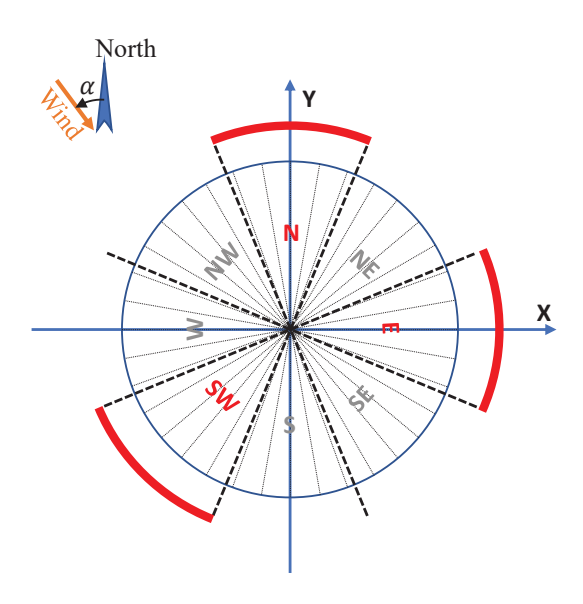


Figure 6: The critical sectors.

for these three sectors. Response parameters considered for performance evaluation were the peak interstory drift  $\hat{Dr}_i$ , residual interstory drift  $\bar{Dr}_i$ , and peak top drift. A total of 400 stochastic wind load samples were considered in each sector with sectoral wind direction variability modeled once again using a uniform probability mass function. Response samples were estimated using both the LSTM metamodel and the high-fidelity OpenSees model from which the sectoral CCDFs were estimated using Eq. (15).

The resulting CCDF are compared in Fig. 8. It is seen that the CCDF by the LSTM metamodel matches remarkably well with the high-fidelity reference. Indeed, the envelope and sectorial CCDFs estimated from the LSTM metamodel overlap those estimated from directly integrating the high-fidelity OpenSees model. This is an expected result since it was shown in Sec. 5.4.1 that the LSTM metamodel is capable of accurately reproducing time history responses of the structural system. It is remarkable to note that the high accuracy holds even for residual interstory drifts, which are challenging to reproduce due to their sensitivity to the accumulation of inelastic deformation. Last, it should be noted that the CCDFs illustrated in Fig. 8 represent a fraction of the information provided by the LSTM metamodel that allows CCDFs to be constructed for any response of interest as it represents a global metamodel of the system (i.e., time history responses at all DOFs are available). This feature makes the LSTM metamodeling framework of this work extremely powerful for

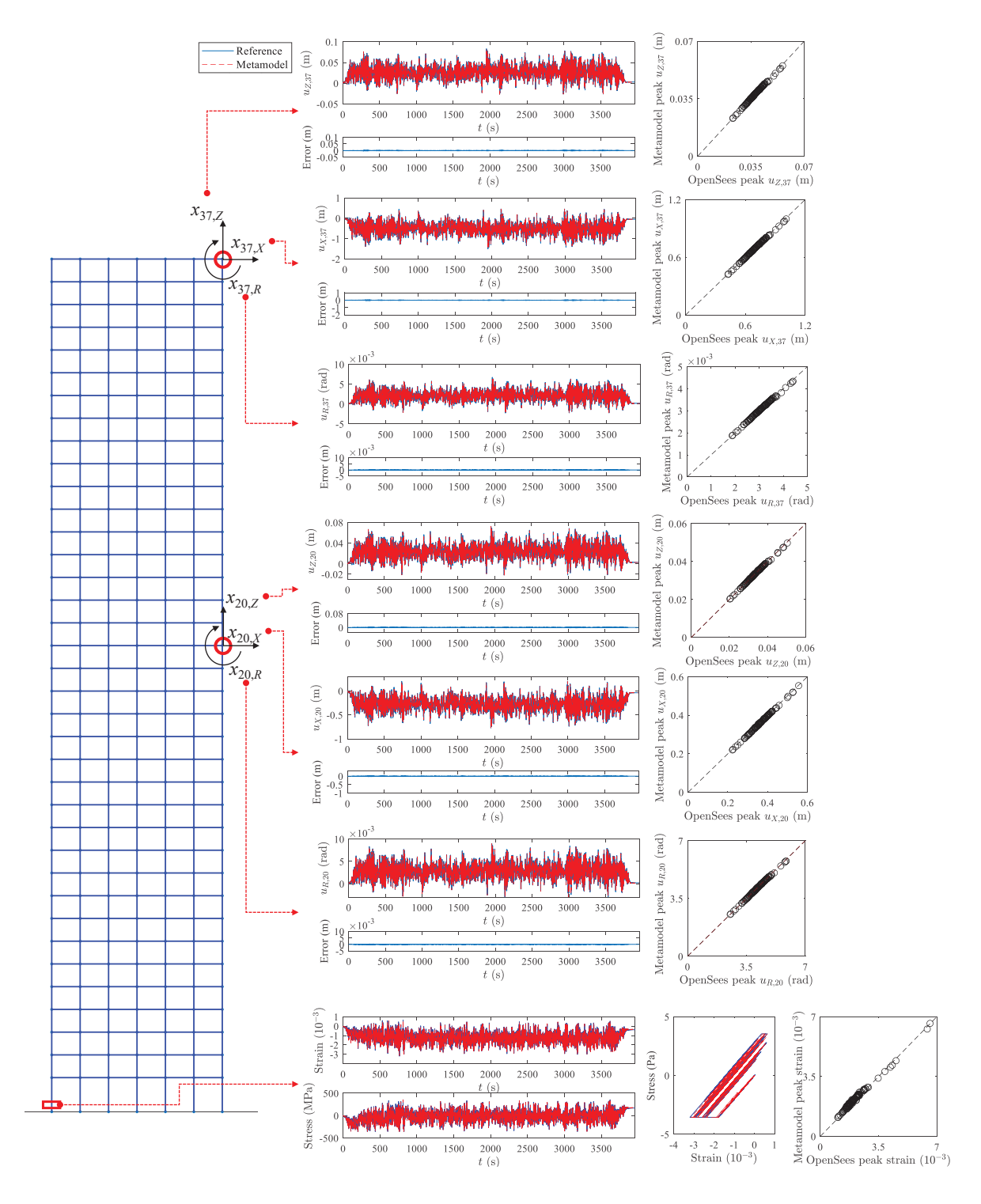


Figure 7: Performance of the trained LSTM metamodel in the critical sectors and a stationary time horizon of  $T=3600~\rm s$ . Example time histories for the East sector and horizontal, vertical, and rotational responses at two locations of the structure as well as the stress and strain fiber response for a column at the base of the structure (corresponding hysteretic curve also shown). Peak values over all three of the critical sectors also shown.

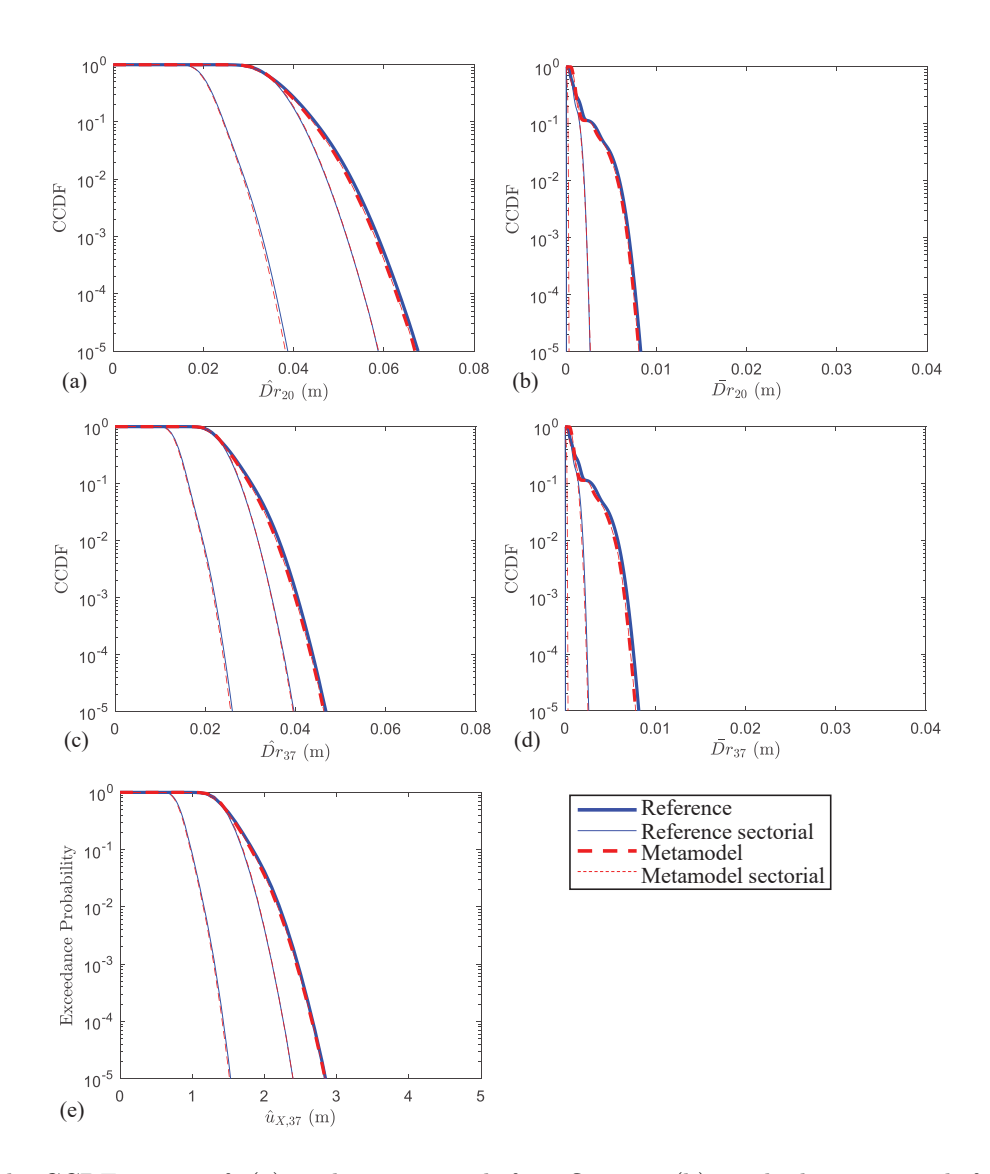


Figure 8: The CCDF curves of: (a) peak interstory drift at floor 20; (b) residual interstory drift at floor 20; (c) peak interstory drift at floor 37; (d) residual interstory drift at floor 37; and (e) peak roof displacement.

general-purpose performance assessments.

Finally, it should be observed that the trained LSTM metamodel was well over 4 orders of magnitude faster at generating the nonlinear response time histories than the high-fidelity OpenSees reference model. This remarkable efficiency coupled with the accuracy demonstrated in this example illustrated the tremendous potential of the proposed approach in applications such as PBWE where uncertainty propagation is essential.

## 6. Summary and Conclusions

This work introduced a framework enabling the rapid intensity-based probabilistic performance assessment of nonlinear and dynamic structural systems subject to stochastic wind excitation. The framework is centered on a deep learning-based response time history metamodeling scheme which entails model order reduction by POD-based Galerkin projection and dynamic behavior learned through LSTM neural networks applied within the reduced space. To address the two key issues of applying such a metamodeling scheme to wind engineering applications, namely the significant variability seen in the wind excitation for different wind directions and the huge computational demand and memory requirements necessary for training LSTM neural networks to long-duration (order of hours) nonlinear dynamic wind response samples, a method is proposed to calibrate the metamodel to data generated for all critical wind directions while considering a reduced wind load duration. The proposed approach is demonstrated on a full-scale fiber-discretized structure subject to stochastic wind loads of one-hour duration causing strong inelasticity. The LSTM metamodel is calibrated to response samples of only a ten-minute duration and is seen to be able to simulate nonlinear time history responses of up to one-hour duration without any accumulation of error. The efficiency gains of the trained LSTM metamodel is seen to be over four orders of magnitude as compared to the high-fidelity modeling environment therefore enabling uncertainty propagation using direct Monte Carlo methods. This is illustrated on the case study where sectorial CCDFs of a range of response parameters of interest, including peak interstory and residual drift, are rapidly estimated with remarkable accuracy. These features demonstrate the immense potential of the proposed scheme for applications in which uncertainty propagation is key, for example, PBWE.

### Acknowledgments

This research effort was supported in part by the National Science Foundation (NSF) under Grant No. 1750339. This support is gratefully acknowledged.

### References

- [1] Jain, A., Srinivasan, M., Hart, G.C.. Performance based design extreme wind loads on a tall building. The structural design of tall buildings 2001;10(1):9–26.
- [2] Ciampoli, M., Petrini, F., Augusti, G., Performance-based wind engineering: towards a general procedure. Structural Safety 2011;33(6):367–378.
- [3] Barbato, M., Petrini, F., Unnikrishnan, V.U., Ciampoli, M.. Performance-based hurricane engineering (pbhe) framework. Structural Safety 2013;45:24–35.
- [4] Beck, A.T., Kougioumtzoglou, I.A., dos Santos, K.R.M.. Optimal performance-based design of non-linear stochastic dynamical RC structures subject to stationary wind excitation. Engineering Structures 2014;78:145–153.
- [5] Spence, S.M.J., Kareem, A.. Performance-based design and optimization of uncertain wind-excited dynamic building systems. Engineering Structures 2014;78:133–144.
- [6] Cui, W., Caracoglia, L.. A unified framework for performance-based wind engineering of tall buildings in hurricane-prone regions based on lifetime intervention-cost estimation. Structural safety 2018;73:75–86.
- [7] Ouyang, Z., Spence, S.M.J.. A performance-based wind engineering framework for envelope systems of engineered buildings subject to directional wind and rain hazards. Journal of Structural Engineering 2020;146(5):04020049.
- [8] Cui, W., Caracoglia, L.. Performance-based wind engineering of tall buildings examining life-cycle downtime and multisource wind damage. Journal of Structural Engineering 2020;146(1).
- [9] Petrini, F., Francioli, M.. Next generation PBWE: Extension of the SAC-FEMA method to high-rise buildings under wind hazards. Structural Safety 2022;99:102255.
- [10] ASCE, Prestandard for performance-based wind design. ASCE Reston, VA; 2019,..

- [11] Muthukumar, S., Baldava, S., Garber, J.. Performance-based evaluation of an existing building subjected to wind forces. In: Advances in hurricane engineering: Learning from our past. 2013, p. 1217–1228.
- [12] Judd, J.P.. Windstorm resilience of a 10-story steel frame office building. ASCE-ASME Journal of Risk and Uncertainty in Engineering Systems, Part A: Civil Engineering 2018;4(3):04018020.
- [13] Mohammadi, A., Azizinamini, A., Griffis, L., Irwin, P.. Performance assessment of an existing 47-story high-rise building under extreme wind loads. Journal of Structural Engineering 2019;145(1):04018232.
- [14] Ouyang, Z., Spence, S.M.J.. Performance-based wind-induced structural and envelope damage assessment of engineered buildings through nonlinear dynamic analysis. Journal of Wind Engineering and Industrial Aerodynamics 2021;208:104452.
- [15] Arunachalam, S., Spence, S.M.J.. Reliability-based collapse assessment of wind-excited steel structures within performance-based wind engineering. Journal of Structural Engineering 2022;148(9):04022132.
- [16] Huang, J., Chen, X.. Inelastic performance of high-rise buildings to simultaneous actions of alongwind and crosswind loads. Journal of Structural Engineering 2022;148(2):04021258.
- [17] Huang, M., Li, Q., Chan, C.M., Lou, W., Kwok, K.C., Li, G.. Performance-based design optimization of tall concrete framed structures subject to wind excitations.

  Journal of Wind Engineering and Industrial Aerodynamics 2015;139:70–81.
- [18] Tabbuso, P., Spence, S.M.J., Palizzolo, L., Pirrotta, A., Kareem, A.. An efficient framework for the elasto-plastic reliability assessment of uncertain wind excited systems. Structural Safety 2016;58:69–78.
- [19] Chuang, W.C., Spence, S.M.J.. An efficient framework for the inelastic performance assessment of structural systems subject to stochastic wind loads. Engineering Structures 2019;179:92–105.

- [20] Huang, J., Chen, X.. Inelastic response of high-rise buildings under strong winds: Accuracy of reduced-order building model and influence of biaxial response interaction. Journal of Structural Engineering 2023;149:04022211.
- [21] Huang, J., Chen, X.. Uncertainty analysis of inelastic response of high-rise buildings to wind using a reduced-order building model. Engineering Structures 2023;288:116224.
- [22] Li, B., Chuang, W.C., Spence, S.M.J.. An adaptive fast nonlinear analysis (AFNA) algorithm for rapid time history analysis. In: 8th ECCOMAS Thematic Conference on Computational Methods in Structural Dynamics and Earthquake Engineering. 2021,.
- [23] Li, B., Chuang, W.C., Spence, S.M.J.. Reliability of inelastic wind excited structures by dynamic shakedown and adaptive fast nonlinear analysis (AFNA). Engineering Structures 2023;296:116869.
- [24] Spiridonakos, M.D., Chatzi, E.N.. Metamodeling of nonlinear structural systems with parametric uncertainty subject to stochastic dynamic excitation. Earthquakes and Structures 2015;8(4):915–934.
- [25] Mai, C.V., Spiridonakos, M.D., Chatzi, E.N., Sudret, B., Surrogate modeling for stochastic dynamical systems by combining nonlinear autoregressive with exogenous input models and polynomial chaos expansions. International Journal for Uncertainty Quantification 2016;6(4).
- [26] Bhattacharyya, B., Jacquelin, E., Brizard, D.. A Kriging-NARX model for uncertainty quantification of nonlinear stochastic dynamical systems in time domain. J Eng Mech 2020;146(7):04020070.
- [27] Chuang, W.C., Spence, S.M.J.. Rapid uncertainty quantification for non-linear and stochastic wind excited structures: a metamodeling approach. Meccanica 2019;54(9):1327–1338.
- [28] Li, B., Chuang, W.C., Spence, S.M.J.. Response estimation of multi-degree-of-freedom nonlinear stochastic structural systems through metamodeling. Journal of Engineering Mechanics 2021;147(11):04021082.

- [29] Kundu, A., Chakraborty, S.. Deep learning-based metamodeling technique for nonlinear seismic response quantification. In: IOP Conference Series: Materials Science and Engineering; vol. 936. IOP Publishing; 2020, p. 012042.
- [30] Zhang, R., Liu, Y., Sun, H.. Physics-informed multi-lstm networks for metamodeling of nonlinear structures. arXiv preprint arXiv:200210253 2020;.
- [31] Zhang, R., Liu, Y., Sun, H.. Physics-guided convolutional neural network (phycnn) for data-driven seismic response modeling. Engineering Structures 2020;215:110704.
- [32] Wang, H., Wu, T.. Knowledge-enhanced deep learning for wind-induced nonlinear structural dynamic analysis. Journal of Structural Engineering 2020;146(11):04020235.
- [33] Zhang, L., Caracoglia, L.. Wind-induced fragility of a monopole structure via artificial neural network based surrogate analysis. Engineering Structures 2023;278:115515.
- [34] Li, B., Spence, S.M.J.. Metamodeling through deep learning of high-dimensional dynamic nonlinear systems driven by general stochastic excitation. Journal of Structural Engineering 2022;148(11):04022186.
- [35] Federal Emergency Management Agency (FEMA), . Seismic performance assessment of buildings, Volume 1 Methodology (FEMA Publication P-58-1). Washington, DC; 2012.
- [36] Irwin, P., Garber, J., Ho, E.. Integration of wind tunnel data with full scale wind climate. In: Proc., 10th Americas Conf. on Wind Engineering. 2005, p. 132–135.
- [37] Isyumov, N., Ho, E., Case, P.. Influence of wind directionality on wind loads and responses. Journal of Wind Engineering and Industrial Aerodynamics 2014;133:169–180.
- [38] Chuang, W.C., Spence, S.M.J.. A framework for the efficient reliability assessment of inelastic wind excited structures at dynamic shakedown. Journal of Wind Engineering and Industrial Aerodynamics 2022;220:104834.
- [39] Arunachalam, S., Spence, S.M.J.. An efficient stratified sampling scheme for the simultaneous estimation of small failure probabilities in wind engineering applications. Structural Safety 2023;101:102310.

- [40] Arunachalam, S., Spence, S.M.J.. Generalized stratified sampling for efficient reliability assessment of structures against natural hazards. Journal of Engineering Mechanics 2023;149:04023042.
- [41] Duarte, T.G.A., Arunachalam, S., Subgranon, A., Spence, S.M.J.. Uncertainty quantification and simulation of wind-tunnel-informed stochastic wind loads. Wind 2023;3(3):375–393.
- [42] Chen, X., Kareem, A.. Proper orthogonal decomposition-based modeling, analysis, and simulation of dynamic wind load effects on structures. Journal of Engineering Mechanics 2005;131(4):325–339.
- [43] Le, T.H., Caracoglia, L.. Reduced-order wavelet-galerkin solution for the coupled, nonlinear stochastic response of slender buildings in transient winds. Journal of Sound and Vibration 2015;344:179–208.
- [44] Mazzoni, S., McKenna, F., Scott, M.H., Fenves, G.L.. OpenSees command language manual. Berkeley, California, United States; 2006.
- [45] ASCE, Minimum design loads and associated criteria for buildings and other structures. ASCE/SEI 7-22; Reston, Virginia; 2022.
- [46] Tokyo polytechnic university (TPU) wind pressure database. 2008. URL: http://wind.arch.t-kougei.ac.jp/system/eng/contents/code/tpu.